ARTICLE

Ab initio Study of the Potential Energy Surface and Product Branching Ratios for Reaction of $O(^1D)$ with C_2H_5Cl

Chong-fu Song[a*], Zhi-mei Tian[a], Quan-xin Li[b], Tian-jing He[b]

a. Department of Chemistry, Fuyang Teacher's College, Fuyang 236041, China
b. Department of Chemical Physics, University of Science and Technology of China, Hefei 230026, China

(Dated: Received on November 12, 2008; Accepted on December 4, 2008)

The potential energy surface of $O(^1D)+C_2H_5Cl$ reaction was studied using QCISD(T)/6-311++G(d,p)//MP2/6-31G(d,p) method. The calculations reveal an insertion-elimination mechanism. The insertion reaction of $O(^1D)$ and C_2H_5Cl produces two energy-rich intermediates, IM1 and IM2, which subsequently decompose into various products. The calculations of the branching ratios of various products formed through the two intermediates were carried out using RRKM (Rice-Ramsperger-Kassel-Marcus) theory at the collision energies of 0, 20.9, 41.8, 62.7, 83.6, 104.5, and 125.4 kJ/mol. HCl is the main decomposition product for IM1; CH_2OH is the main decomposition product for IM2. Since IM1 is more stable than IM2, HCl is probably the main product of the $O(^1D)+C_2H_5Cl$ reaction.

Key words: C_2H_5Cl, Branching ratio, Rate constant

I. INTRODUCTION

Incineration is the cleanest method for disposal of chlorinated hydrocarbons (CHCs). At typical feel-lean combustion conditions, the reactions of halogenated alkyls with oxygen atoms are important in the oxidation process of polyhalogenated hydrocardons. Halogenated alkanes can also undergo photodecomposition to halogenated alkyl radicals. The reaction of halogenated alkyl radicals with O atoms is known to produce halogenerated aslkoxy radicals, which play an important role in stratospheric ozone depletion [1]. Furthermore, their wide use as refrigerants, aerosol spray propellants, solvents, and in foam packing made them one of the major constituents of man-made greenhouse gases with potential implications for global warming [2]. Thus, numerous studies have been devoted to the theoretical and experimental investigation of the properties of these compounds [3-14]. To incinerate industrial waste CHCs in a more efficient and less hazardous way, it is necessary to further investigate this kind of combustion process. It is especially important to understand the incineration mechanism, specific pathways, and rate con-stants for important elementary reactions.

The potential energy surface of C_2H_5Cl+OH reaction has been studied by Wang *et al.* using *ab initio* molecular orbital theory with several basis sets and at several levels of theory [1]. Li *et al.* obtained the potential energy surface of $H+C_2H_5Cl$ using PMP4(SDTQ)/6-311+G(3df,2p)//MP2/6-311G(d,p) method and got the rate constants of various channels by canonical variational transition state theory [15]. He *et al.* studied the hydrogen/deuterium abstraction from C_2H_5Cl/C_2D_5Cl with chlorine atom at G3//MP2/6-311G(d,p) [16]. Alagia *et al.* have studied the reactive properties of $O(^1D)+CF_3Br$ using crossed molecular beam scattering measurements and quasiclassical trajectory calculations [17]. The reaction of $O(^1D)+SiH_4$ has been investigated by Nguyen *et al.* [18]; they obtained the ground state potential energy surface by CCSD(T)/6-311+G(3df,2p) method and got the product branching ratios using RRKM (Rice-Ramsperger-Kassel-Marcus) theory. He *et al.* have studied the potential energy surface for the decomposition of CH_3OCl using G2MP2 method [19].

Sun *et al.* have studied the ground state potential energy surface of $O(^1D)+C_2H_6$ using CCSD(T)/6-311+G(3df,2p)//B3LYP/6-311G(d,p) method and studied the product branching ratios using RRKM theory [20]. They found that C_2H_5OH formed in the reaction. They did not consider the spin coupling between the two reactions $O(^1D)+C_2H_6$ and $O(^3P)+C_2H_6$. To date, no direct theory or experimental studies of $O(^1D)+C_2H_5Cl$ have been reported. In the work, *ab initio* calculations based on QCISD(T)/6-311++G(d,p)//MP2/6-31G(d,p) method were performed to explore ground state on the potential energy surface of the $O(^1D)+C_2H_5Cl$. The branching ratios of various products formed through two intermediates were carried out using RRKM theory at the collision energies of 20.9, 41.8, 62.7, 83.6, 104.5, and 125.4 kJ/mol.

*Author to whom correspondence should be addressed. E-mail: songcf@mail.ustc.edu.cn

II. COMPUTATIONAL DETAILS

Geometries of the reactants, products, intermediates, and transition states were optimized at the second-order Moller-Plesset perturbation MP2/6-31G(d,p) level of theory. Vibrational frequencies, also calculated at the MP2/6-31G(d,p) level, were used to characterize stationary points, zero-point energy (ZPE) corrections, and rate constant calculations. The numbers of imaginary frequencies for intermediates and transition states are 0 and 1, respectively. All the tight transition states are verified by the internal reaction coordinate (IRC) calculations. The ZPE and vibrational frequencies calculated at this level are scaled by a factor of 0.9370 [21]. The energies of the stationary points are refined at the QCISD(T)/6-311++G(d,p) level. All the calculations were carried out using the Gaussian 03 suite of programs [22].

The energy-dependent rate constants for individual unimolecular reaction steps were computed using RRKM theory [23]. For a unimolecular reaction

$$\mathrm{R}^* \rightarrow \mathrm{R}^{\neq} \rightarrow \mathrm{P} \tag{1}$$

where R^* is the energized reactant, $\mathrm{R}^{\neq}$ is the activated complex or transition state on the potential energy surface, and P represents the product. The microcanonical rate constant, $k(E)$, according to RRKM theory can be expressed as:

$$k(E) = \left(\frac{I^{\neq}}{I}\right)^{1/2} \frac{\sigma}{h} \frac{W^{\neq}(E - E^{\neq})}{\rho(E)} \tag{2}$$

here, σ is the reaction path degeneracy, h is Plank's constant, $W^{\neq}(E - E^{\neq})$ denotes the total number of states of the transition state with activation energy (barrier height) $E^{\neq}$, and $\rho(E)$ represents the density of states of the energized reaction molecule. $I^{\neq}$ and I are the overall moments of inertia for transition states and IM1 (or IM2), respectively. The direct count method [23] is used to calculate the $W^{\neq}(E - E^{\neq})$ and $\rho(E)$ values in this work. The total available internal energy E is taken as the energy of chemical activation (e.g., the energy released in the $O(^1D)+C_2H_5Cl \rightarrow$IM reaction) plus a collision energy, E_{col}.

For the bond-cleavage channels, the microcanonical variational transition state theory (MVTST) is employed [24]. The position of the transition state is determined based on the following criterion:

$$\frac{\partial W^{\neq}\left(E - E^{\neq}\right)}{\partial R_{\mathrm{C}}} = 0 \tag{3}$$

where $W^{\neq}(E - E^{\neq})$ is the number of states and R_{C} is the reaction coordinate. The reaction coordinate is chosen as the length of the breaking bond. The geometry at the R_{C} that minimizes the number of states is the transition state. The MP2/6-31G(d,p) method is used to scan the PES along the reaction coordinates and to compute corresponding $3N-7$ vibrational frequencies projected out of the gradient direction. The energies of the partially optimized structures are then refined at the QCISD(T)/6-311++G(d,p) level.

III. RESULTS AND DISCUSSION

The optimized geometries of various stationary points are presented in Fig.1 along with the available experimental data [25-29]. The calculated geometries of C_2H_5Cl, HCl, H_2, and H_2O are in good agreement with the corresponding experimental values. Table I shows the moments of inertia and scaled vibrational frequencies of the intermediates and transition states obtained directly by MP2/6-31G(d,p) method. Table II contains energies and molecular parameters for variational transition states obtained using the MVTST approach. The schematic potential energy profile of the $O(^1D)+C_2H_5Cl$ based on QCISD(T)/6-311++G(d,p) energies with ZPE corrections at the MP2/6-31G(d,p) level are depicted in Fig.2. Unless otherwise stated, the energy differences below are all at the QCISD(T) level with ZPE corrections at the MP2/6-31G(d,p) level.

A. Potential energy surface and reaction mechanism

As shown in Fig.2, a typical insertion-elimination mechanism for the reaction of $O(^1D)$ with C_2H_5Cl is revealed. The $O(^1D)+C_2H_5Cl$ reaction is largely exothermic and occurs without an entrance barrier. Two intermediates, IM1 and IM2, are formed in the reaction of $O(^1D)$ and C_2H_5Cl. The distances of newly formed C−O bonds in IM1 and IM2 are 1.392 and 1.422 Å, respectively. The distances of H−O bonds in IM1 and IM2 are 0.967 and 0.964 Å, respectively. The energies of IM1 and IM2 are 604.0 and 575.2 kJ/mol, respectively, lower than the reactants $O(^1D)+C_2H_5Cl$. So IM1 and IM2 should be highly chemical activated complexes, and can undergo various possible production channels. Eleven production channels of IM1 and eight production channels of IM2 were found and will be discussed separately following the energetic sequence.

1. Decomposition of IM1

The energetically most favourable reaction path is IM1$\rightarrow CH_3CHO+HCl$ via a four-membered ring transition state TS1. The breaking C2−Cl4 and O3−H5 bonds lengths are 2.628 and 1.035 Å, respectively. The forming H5−Cl4 bond length of 1.962 Å is 0.693 Å longer than the equilibrium distance of the HCl molecule. The barrier height is 168.5 kJ/mol. The overall reaction of $O(^1D)+C_2H_5Cl \rightarrow CH_3CHO+HCl$ is highly exothermic by 584.8 kJ/mol.

DOI:10.1088/1674-0068/22/01/87-96

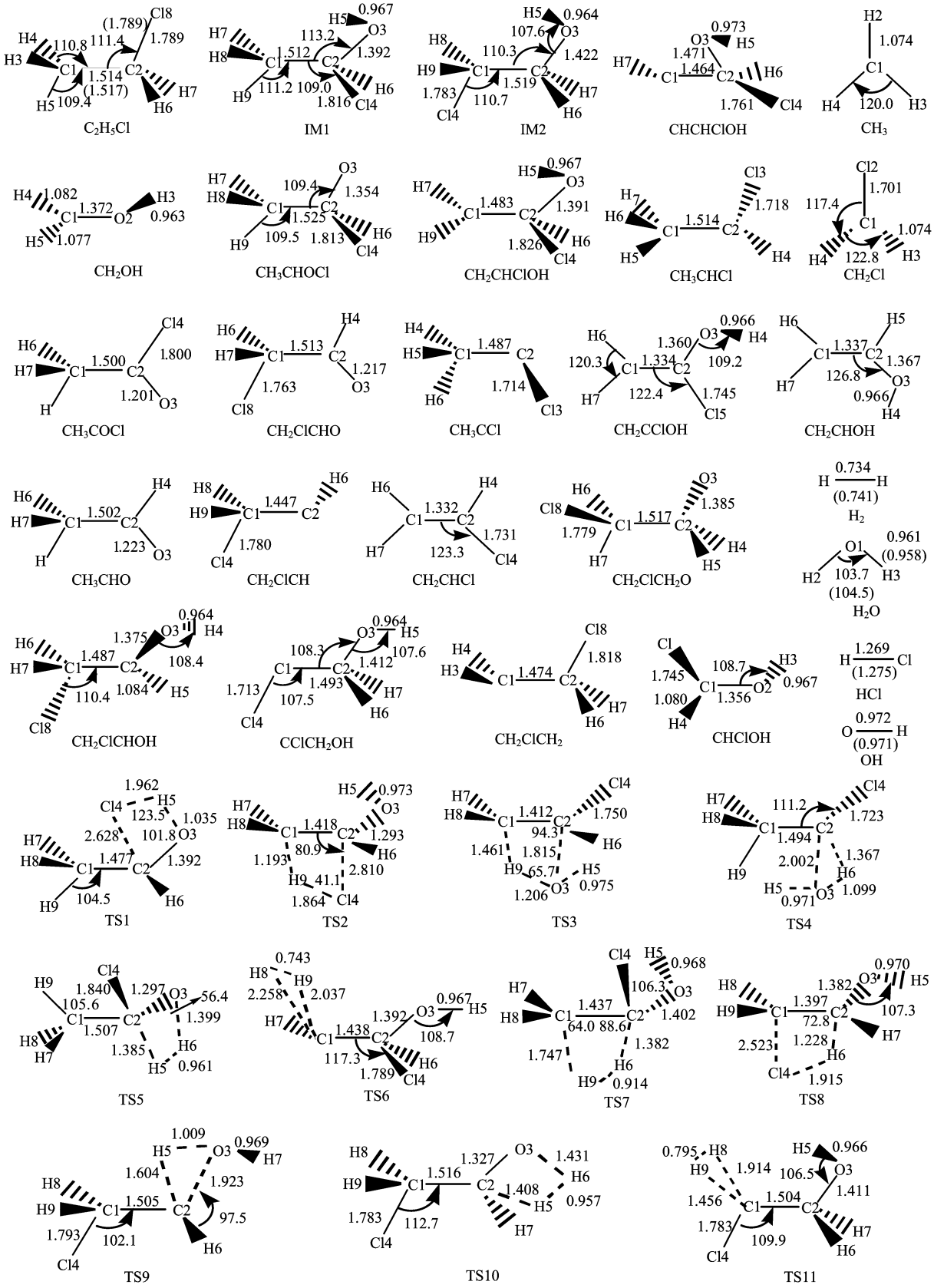

FIG. 1 Optimized geometries of reactants, intermediates, products, and eleven transition states at the MP2/6-31G(d,p) level of theory. The values in parentheses are the experimental values [25-29]. Bond lengths are in Å and the angles are in (°).

DOI:10.1088/1674-0068/22/01/87-96

TABLE I Scaled vibrational frequencies, moments of inertia (I_A, I_B, I_C) of molecular species at MP2/6-31G(d,p) level of theory.

Species	I_A, I_B, $I_C/10^{-46}$ kg·m^2	Vibrational frequencies[a]/cm^{-1}
IM1	9.5, 18.2, 25.4	272.7, 315.6, 328.6, 427.4, 457.6, 635.3, 884.7, 998.6, 1045.6, 1118.8, 1236.5, 1286.6, 1360.6, 1380.4, 1446.3, 1451.8, 2939.4, 3018.9, 3036.6, 3048.7, 3613.6
IM2	2.9, 34.6, 36.2	135.6, 231.7, 298.3, 377.9, 755.8, 769.9, 993.5, 1029.9, 1046.5, 1103.1, 1244.6, 1265.9, 1325.6, 1364.1, 1448.7, 1471.7, 2929.1, 2974.6, 3016.5, 3051.5, 3650.3
TS1	9.9, 19.2, 25.4	−362.3, 159.9, 182.3, 337.7, 357.4, 388.8, 399.3, 414.4, 537.9, 600.1, 830.6, 844.4, 1003.3, 1089.9, 1151.2, 1177.7, 1366.4, 2605.2, 2909.0, 3614.4, 4150.1
TS2	10.1, 17.7, 25.9	−1537.6, 257.2, 271.3, 372.1, 420.0, 470.7, 509.6, 640.6, 853.4, 923.7, 1019.5, 1096.8, 1184.1, 1243.7, 1336.8, 1397.7, 1488.9, 2181.3, 3001.4, 3145.3, 3604.0
TS3	9.4, 18.6, 25.8	−2091.2, 241.0, 321.9, 350.2, 480.0, 577.0, 654.0, 911.0, 938.2, 1003.6, 1050.1, 1110.8, 1350.5, 1418.8, 1433.5, 1443.0, 1995.3, 2221.3, 2947.0, 3048.0, 3064.5
TS4	9.5, 22.9, 30.0	−633.0, 218.4, 253.7, 273.6, 423.0, 641.9, 816.0, 875.8, 1029.9, 1079.7,1255.6, 1341.9, 1368.4, 1398.6, 1424.9, 1541.9, 2525.8, 2893.5, 3027.2, 3032.6, 3103.6
TS5	9.1, 28.6, 34.9	−929.4, 114.6, 228.8, 341.6, 395.5, 474.0, 737.1, 942.4, 989.1, 1038.2, 1149.9, 1262.3, 1309.1, 1374.3, 1418.8, 1499.5, 1786.2, 3010.7, 3104.0, 3119.5, 3542.5
TS6	9.5, 19.7, 26.5	−1956.4, 232.1, 287.3, 382.8, 515.8, 532.9, 596.6, 666.3, 801.8, 843.1, 1014.9, 1078.4, 1204.7, 1313.2, 1393.2, 1446.6, 1606.3, 3038.9, 3080.5, 3136.8, 3530.1
TS7	11.4, 19.5, 28.7	−1007.5, 200.6, 217.9, 259.8, 366.6, 400.9, 537.0, 701.3, 729.6, 921.1, 1061.3, 1083.9, 1345.4, 1418.6, 1440.4, 1495.2, 2035.6, 2915.8, 3001.0, 3026.9, 3593.0
TS8	7.6, 30.1, 34.9	−1438.8, 70.1, 214.0, 308.3, 362.3, 447.6, 718.9, 886.6, 951.9, 1023.0, 1072.4, 1159.9, 1225.4, 1296.2, 1367.1, 1456.8, 1735.0, 3068.3, 3076.4, 3184.6, 3567.6
TS9	3.0, 38.3, 40.1	−514.2, 100.1, 167.3, 238.9, 339.3, 369.0, 661.7, 725.8, 885.1, 995.7, 1046.4, 1066.7, 1216.3, 1258.6, 1467.5, 1529.2, 2932.8, 2956.8, 2973.9, 3035.0, 3624.3
TS10	3.0, 33.8, 35.3	−2030.2, 142.5, 234.6, 397.7, 619.2, 769.4, 884.0, 942.0, 980.3, 1050.0, 1160.9, 1224.3, 1233.9, 1341.0, 1397.4, 1426.1, 1956.1, 2259.6, 2855.6, 2982.5, 3062.3
TS11	3.4, 33.6, 35.2	−790.8, 157.9, 243.8, 347.0, 393.4, 477.9, 490.9, 751.7, 799.7, 819.6, 961.0, 1051.1, 1099.1, 1176.7, 1284.5, 1348.8, 1420.1, 2850.0, 2985.5, 3261.1, 3624.9

[a]Vibrational frequency is scaled by a factor of 0.9370 [21].

The second decomposition path of IM1 produces CH_2CHOH+HCl via transition state TS2, located about 198.1 kJ/mol higher. TS2 is a four-member-ring structure. The breaking C1−H9 and C2−Cl4 bonds are elongated to 1.193 and 2.810 Å, respectively. The forming H9−Cl4 bond is 1.864 Å. The production of CH_2CHOH+HCl is exothermic by 534.2 kJ/mol for the reaction of $O(^1D)$+C_2H_5Cl.

The third reaction channel of IM1 is the formation of CH_2CHCl+H_2O via transition state TS3 over a barrier of 307.2 kJ/mol. TS3 is a four-membered ring transition state. The breaking C2−O3 and C1−H9 bonds are 1.815 and 1.461 Å, respectively. The forming H9−O3 bond is 1.206 Å. The CH_2CHCl+H_2O product channel is 539.6 kJ/mol exothermic with respect to $O(^1D)$+C_2H_5Cl.

The IM1→CH_3CCl+H_2O channel occurs through a three-centered transition state TS4. The breaking C2−O3 and C2−H6 bonds are 2.002 and 1.367 Å, respectively. The distance of the forming O3−H6 is 1.099 Å. The barrier height of the process is 328.5 kJ/mol, and the overall process of this channel ($O(^1D)$+C_2H_5Cl→CH_3CCl+H_2O) is exothermic by 308.1 kJ/mol.

The fifth decomposition path of IM1 is the production of CH_3COCl+H_2 via the four-member-ring transition state TS5 with an energy barrier of 362.8 kJ/mol. The forming H5−H6 bond is 0.961 Å long, which is 0.227 Å longer than the equilibrium distance of the H_2 molecule. The production channel of CH_3COCl+H_2 is exothermic by 572.2 kJ/mol with respect to $O(^1D)$+C_2H_5Cl.

The sixth channel of the decomposition of IM1 is the 1,1-elimination of H_2 forming CHCHClOH+H_2 via transition state TS6. TS6 is a three-member-ring structure. The forming H8−H9 is 0.743 Å long, which is only 0.009 Å longer than the equilibrium bond length of the H_2 molecule. The breaking C1−H8 and C1−H9 is stretched as long as 2.258 and 2.037 Å, respectively. The corresponding barrier height of this process is 456.5 kJ/mol. The formation of CHCHClOH+H_2 of IM1 is endothermic by 459.4 kJ/mol, but the overall process of $O(^1D)$+C_2H_5Cl→CHCHClOH+H_2 is

DOI:10.1088/1674-0068/22/01/87-96

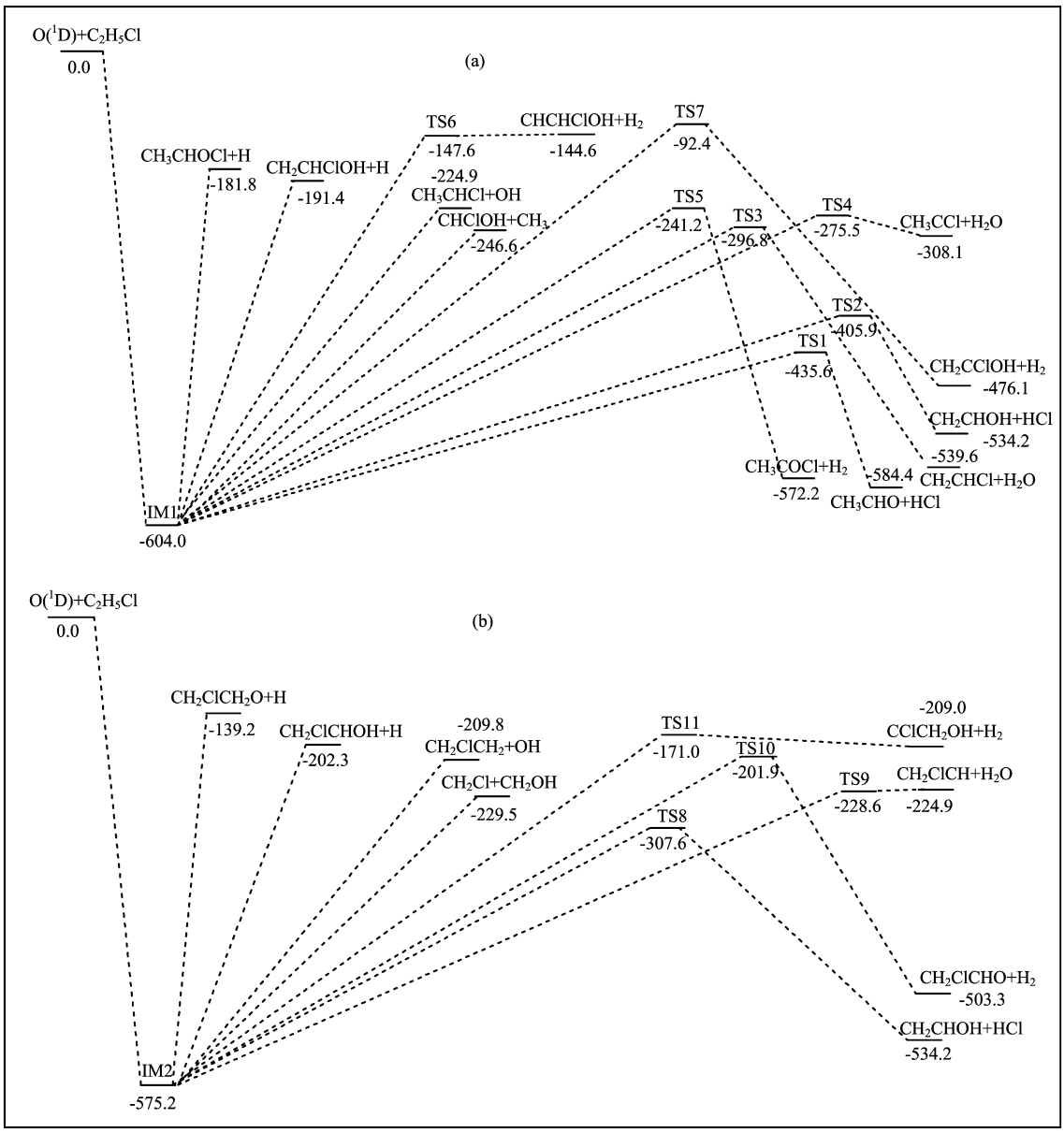

FIG. 2 The ground state potential energy surface of reaction O(^{1}D)+C_2H_5Cl calculated at the QCISD(T)/6-311++G(d,p)//MP2/6-31G(d,p) level. The energy is in unit of kJ/mol.

exothermic by 144.6 kJ/mol.

The seventh channel is the 1,2-elimination of H_2 to $CH_2CClOH+H_2$ through a four-membered ring transition state TS7. The forming H6−H9 bond length is 0.914 Å, and the breaking C1−H9 and C2−H6 bonds are 1.747 and 1.382 Å, respectively. The barrier height of the process is as high as 511.6 kJ/mol. The $CH_2CClOH+H_2$ production channel is exothermic by 476.1 kJ/mol with respect to O(^{1}D)+C_2H_5Cl.

The last four channels are all single bond fission processes without well-defined transition states. The O−H, C−H, C−C, and C−O bond fissions of IM1 produce $CH_3CHOCl+H$, $CH_2CHClOH+H$, $CHClOH+CH_3$, and $CH_3CHCl+OH$, respectively. These channels are endothermic relative to IM1 by 422.2, 412.6, 357.4, and 379.1 kJ/mol, respectively. The corresponding transition states were located by MVTST introduced above, and the parameters are listed in Table II.

2. Decomposition of IM2

The most feasible decomposition channel of IM2 is the formation of $CH_2CHOH+HCl$ via transition state TS8. TS8 is a four-membered ring structure. The breaking C1−Cl4 and C2−H6 are lengthened to 2.523 and 1.228 Å, respectively. The distance of forming H6−Cl4 is 1.915 Å. The barrier

DOI:10.1088/1674-0068/22/01/87-96

TABLE II Energies and molecular parameters for variational transition states obtained using the MVTST approach[a].

Species	R_c[b]	Energy[c]	I_A, I_B, $I_C/10^{-46}$ kg·m^2	Vibrational frequencies[d]/cm^{-1}
$CH_3CHClO-H$	2.5	415.1[e]	9.9, 18.6, 24.9	−808.8, 263.2, 286.9, 325.4, 409.9, 430.3, 513.8, 640.3, 868.0, 951.4, 1026.9, 1101.3, 1158.1, 1177.8, 1349.4, 1433.6, 1439.5, 2850.2, 2921.1, 3027.3, 3050.0
$CH_2CHClOH-H$	2.7	389.2[e]	10.0, 19.4, 25.3	−755.3, 323.1, 335.6, 362.4, 435.6, 506.4, 530.3, 536.7, 623.8, 771.3, 934.4, 1018.5, 1098.4, 1204.7, 1223.3, 1345.7, 1414.2, 2942.5, 3030.7, 3148.9, 3542.8
$CH_3CHCl-OH$	3.1	389.2[e]	14.3, 25.6, 36.7	−298.1, 74.9, 185.6, 226.3, 321.8, 408.2, 651.0, 772.3, 857.6, 976.5, 1076.6, 1141.1, 1256.2, 1376.0, 1433.2, 1450.7, 2892.5, 2971.4, 3006.3, 3036.0, 3202.8
$CH_3-CHClOH$	2.7	304.3[e]	14.3, 24.0, 35.6	−287.4, 43.4, 152.3, 239.9, 367.3, 450.7, 487.4, 512.6, 721.4, 796.8, 910.5, 1120.0, 1226.3, 1331.0, 1393.5, 1395.3, 2985.6, 3084.3, 3149.7, 3154.3, 3607.3
CH_2ClCH_2O-H	2.4	436.0[f]	3.4, 34.2, 36.0	−715.7,176.2, 279.4, 425.5, 493.0, 635.2, 751.5, 815.4, 961.1, 1001.8, 1023.8, 1047.9, 1124.1, 1209.8, 1310.8, 1367.3, 1395.9, 2420.7, 2844.6, 2915.1, 3019.6
$CH_2ClCHOH-H$	2.7	361.6[f]	3.8, 34.3, 36.2	−718.8, 142.2, 248.4, 386.0, 419.9, 452.3, 488.8, 748.8, 777.8, 923.5, 1010.7, 1125.8, 1162.3, 1198.2, 1263.7, 1401.3, 1434.1, 2931.9, 3020.0, 3028.6, 3623.9
CH_2ClCH_2-OH	2.8	361.6[f]	3.7, 51.6, 54.0	−256.1, 62.6, 113.8, 139.0, 308.0, 473.1, 612.1, 644.8, 760.5, 868.7, 1052.0, 1079.2, 1231.1, 1237.0, 1432.2, 1458.4, 3001.1, 3029.7, 3072.0, 3138.6, 3523.4
CH_2OH-CH_2Cl	2.9	316.8[f]	5.5, 53.9, 55.5	−252.5, 29.4, 114.8, 184.7, 354.3, 405.3, 562.9, 680.1, 811.1, 888.0, 1002.3, 1030.6, 1159.2, 1309.8, 1398.8, 1452.1, 2988.3, 3040.4, 3126.1, 3168.8

[a] Transition states obtained using MVTST for bond-breaking, barrierless channels at E_{col} of 0-125.4 kJ/mol.
[b] R_C: Breaking bond distance in unit of Å.
[c] Barrier energy is in unit of kJ/mol.
[d] Vibrational frequency is scaled by a factor of 0.9370 [21].
[e] The energy is relative to IM1.
[f] The energy is relative to IM2.

height is calculated as 267.5 kJ/mol. The overall process of the $O(^1D)+C_2H_5Cl\rightarrow IM2\rightarrow CH_2CHOH+HCl$ is exothermic by 534.2 kJ/mol.

The second decomposition pathway of IM2 is the production of $CH_2ClCH+H_2O$ via a three-centered transition state TS9. The corresponding barrier height is 346.5 kJ/mol. The breaking C2−H5 and C2−O3 bonds are 1.604 and 1.923 Å, respectively. The forming H5−O3 bond is 1.099 Å, which is 0.138 Å longer than the equilibrium bond length of OH in H_2O molecule. The H_2O fragment in TS9 looks like the H_2O molecule. Consequently, TS9 is a very late, product-like tran-sition state. At the QCISD(T)/6-311++G(d,p) level TS9 lies 3.8 kJ/mol lower in energy than the $CH_2ClCH+H_2O$ products, indicating that this reaction channel most likely does not have an exit barrier. The production of $CH_2ClCH+H_2O$ is exothermic by 224.9 kJ/mol with respect to $O(^1D)+C_2H_5Cl$.

The third decomposition path of IM2 is 2,3-elimination process to $CH_2ClCHO+H_2$ through the four-member-ring transition state TS10 with a barrier of 373.3 kJ/mol. The breaking C2−H5 and O3−H6 bonds are 1.408 and 1.431 Å, respectively. The forming H5−H6 bond is 0.957 Å. The overall process is exothermic by 503.3 kJ/mol with respect to the $O(^1D)+C_2H_5Cl$.

Another three-center decomposition of IM2 produces $CClCH_2OH+H_2$ via transition state TS11 over a barrier of 404.2 kJ/mol. The breaking C1−H8 and C1−H9 bonds are 1.914 and 1.456 Å, respectively. The forming H8−H9 bond is 0.795 Å. The formation of $CClCH_2OH+H_2$ is endothermic by 366.2 kJ/mol, however, the overall process of $O(^1D)+C_2H_5Cl\rightarrow IM2\rightarrow CClCH_2OH+H_2$ is exothermic by 209.0 kJ/mol.

The last four channels are all single bond fission pathways without well-defined transition states. The O−H, C−H, C−O, and C−C bond fissions of IM2 produce CH_2ClCH_2O+H, $CH_2ClCHOH+H$, CH_2ClCH_2+OH, and CH_2OH+CH_2Cl, respectively. These channels are endothermic relative to IM2 by 436.0, 372.9, 365.3, and

DOI:10.1088/1674-0068/22/01/87-96

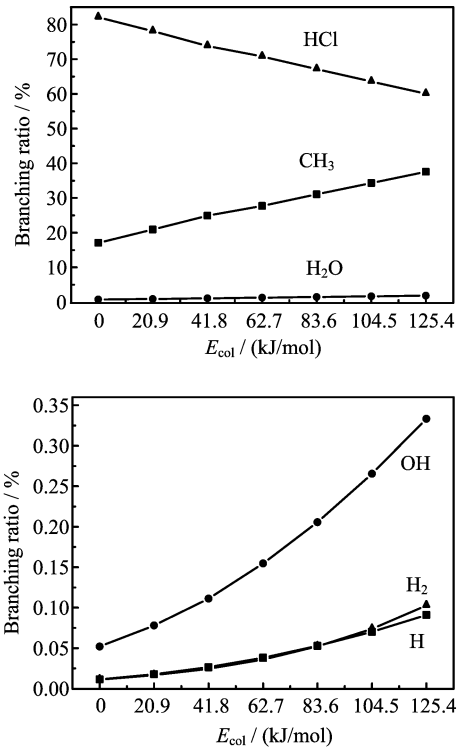

FIG. 3 Calculated branching ratios of the products of unimolecular decomposition of IM1 at collision energies of 0-125.4 kJ/mol.

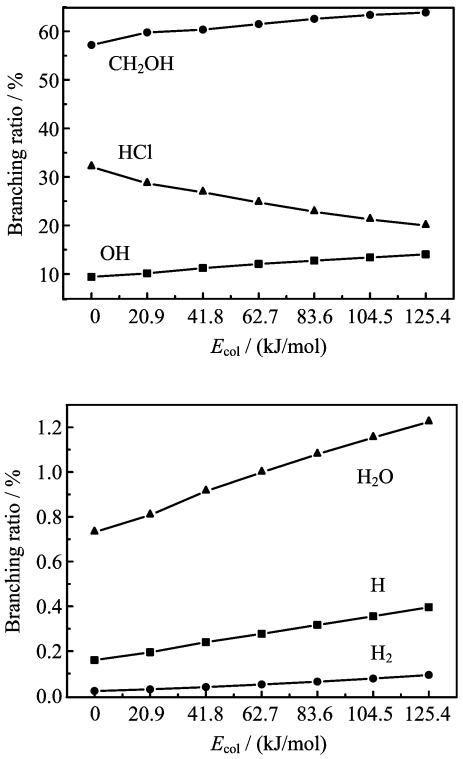

FIG. 4 Calculated branching ratios of the products of unimolecular decomposition of IM2 at collision energies of 0-125.4 kJ/mol.

345.7 kJ/mol, respectively. The corresponding transition states were located by MVTST introduced above, and the parameters are listed in Table II.

B. Energy-dependent rate constants and product branching ratios

The energy-dependent rate constants and the branching ratios for the decomposition channels at the collision energy of E_{col}=0, 20.9, 41.8, 62.7, 83.6, 104.5, and 125.4 kJ/mol for the decompositions of IM1 and IM2 are collected in Table III and Table IV, respectively. Then, we get the graphs of the branching ratios for the H, OH, CH_3, H_2, H_2O, and HCl formation channels of IM1 and the H, OH, CH_2OH, H_2, H_2O, and HCl formation channels of IM2 as a function of collision energies which are depicted in Fig.3 and Fig.4, respectively.

In the decomposition of the chemical activated complex IM1, the HCl formation channels of IM1 were found to have the highest rate constant in the range of 10^{11} s^{-1}, while H and H_2 formation channels which have almost the same rate constant have the lowest rate constant which is 2-3 orders of magnitude lower than the HCl formation channels. The rate constant of the OH formation channel (IM1→CH_3CHCl+OH) is a little larger than the H and H_2 formation channels. The rate constants of the formations CH_3 and H_2O are both between those of the formations of H_2 and HCl. From Fig.3, we can see that the branching ratio of the formation of HCl is the highest (82.1% at E_{col}=0) followed by CH_3 (17.1%). Therefore, for the collision energy of 0, the major products are HCl and CH_3 with the branching ratio of about 4.8:1 between them. The branching ratios of the formations of H, H_2, H_2O, OH, and CH_3 increase with the collision energy except for that of HCl, which decreases with the collision energy. The branching ratios of H, H_2, and OH change from 0.01%, 0.01%, and 0.05% to 0.09%, 0.10%, and 0.33%, respectively, but these channels remain minor ones. However, the branching ratio of the formation of HCl decreases from 82.1% to 60.1% when E_{col} changes from 0 to 125.4 kJ/mol. It is obvious in Fig.3 that the formations of HCl and CH_3 become competing as the collision energy increases. At a collision energy of 125.4 kJ/mol, the branching ratios of HCl and CH_3 are 60.1% and 37.6%, respectively, with the branching ratio of 1.6:1 between them. To summarize, the main product of the decomposition of IM1 is HCl followed by CH_3, and CH_3 competes with HCl at higher collision energy. H_2O, H, H_2, and OH are minor products.

According to Table IV, for the decomposition of IM2, the formation channel of CH_2OH has the highest rate constant k_{15} which is in the range of 10^{11} s^{-1} followed by the formation channel of HCl, while the H_2 formation channel has the lowest rate constant which is in the

DOI:10.1088/1674-0068/22/01/87-96

TABLE III Microcanonical rate constants and branching ratios of the decompositions of IM1 for collision energies 0-125.4 kJ/mol.

E_{col}	Rate constant/s^{-1}	Branching ratio/%	E_{col}	Rate constant/s^{-1}	Branching ratio/%
	IM1 $\xrightarrow{k_1}$ $CH_3CHOCl+H$			IM1 $\xrightarrow{k_7}$ $CH_3COCl+H_2$	
0	1.28×10^{7}	1.69×10^{-3}	0	7.16×10^{7}	9.48×10^{-3}
20.9	2.80×10^{7}	2.91×10^{-3}	20.9	1.25×10^{8}	1.30×10^{-2}
41.8	5.67×10^{7}	4.67×10^{-3}	41.8	2.09×10^{8}	1.72×10^{-2}
62.7	1.08×10^{8}	7.20×10^{-3}	62.7	3.34×10^{8}	2.23×10^{-2}
83.6	1.94×10^{8}	1.05×10^{-2}	83.6	5.16×10^{8}	2.78×10^{-2}
104.5	3.34×10^{8}	1.47×10^{-2}	104.5	7.73×10^{8}	3.40×10^{-2}
125.4	5.51×10^{8}	1.99×10^{-2}	125.4	1.13×10^{9}	4.08×10^{-2}
	IM1 $\xrightarrow{k_2}$ $CH_2CHClOH+H$			IM1 $\xrightarrow{k_8}$ $CH_2CHCl+H_2O$	
0	7.22×10^{7}	9.56×10^{-3}	0	2.59×10^{9}	3.43×10^{-1}
20.9	1.43×10^{8}	1.49×10^{-2}	20.9	3.91×10^{9}	4.07×10^{-1}
41.8	2.65×10^{8}	2.18×10^{-2}	41.8	5.74×10^{9}	4.72×10^{-1}
62.7	4.66×10^{8}	3.11×10^{-2}	62.7	8.19×10^{9}	5.46×10^{-1}
83.6	7.83×10^{8}	4.23×10^{-2}	83.6	1.14×10^{10}	6.15×10^{-1}
104.5	1.26×10^{9}	5.55×10^{-2}	104.5	1.55×10^{10}	6.82×10^{-1}
125.4	1.97×10^{9}	7.11×10^{-2}	125.4	2.07×10^{10}	7.47×10^{-1}
	IM1 $\xrightarrow{k_3}$ $CH_3CHCl+OH$			IM1 $\xrightarrow{k_9}$ CH_3CCl+H_2O	
0	3.92×10^{8}	5.19×10^{-2}	0	3.03×10^{9}	4.01×10^{-1}
20.9	7.50×10^{8}	7.81×10^{-2}	20.9	4.83×10^{9}	5.03×10^{-1}
41.8	1.35×10^{9}	1.11×10^{-1}	41.8	7.42×10^{9}	6.11×10^{-1}
62.7	2.32×10^{9}	1.55×10^{-1}	62.7	1.10×10^{10}	7.33×10^{-1}
83.6	3.81×10^{9}	2.06×10^{-1}	83.6	1.60×10^{10}	8.63×10^{-1}
104.5	6.03×10^{9}	2.65×10^{-1}	104.5	2.25×10^{10}	9.90×10^{-1}
125.4	9.23×10^{9}	3.33×10^{-1}	125.4	3.10×10^{10}	1.12
	IM1 $\xrightarrow{k_4}$ $CHClOH+CH_3$			IM1 $\xrightarrow{k_{10}}$ $CH_2CHOH+HCl$	
0	1.29×10^{11}	17.1	0	3.63×10^{11}	48.1
20.9	2.01×10^{11}	20.9	20.9	4.47×10^{11}	46.5
41.8	3.03×10^{11}	24.9	41.8	5.43×10^{11}	44.7
62.7	4.16×10^{11}	27.7	62.7	6.53×10^{11}	43.5
83.6	5.76×10^{11}	31.1	83.6	7.75×10^{11}	41.8
104.5	7.80×10^{11}	34.3	104.5	9.11×10^{11}	40.1
125.4	1.04×10^{12}	37.6	125.4	1.06×10^{12}	38.3
	IM1 $\xrightarrow{k_5}$ $CHCHClOH+H_2$			IM1 $\xrightarrow{k_{11}}$ $CH_3CHO+HCl$	
0	1.16×10^{7}	1.54×10^{-3}	0	2.57×10^{11}	34.0
20.9	3.40×10^{7}	3.54×10^{-3}	20.9	3.03×10^{11}	31.5
41.8	8.81×10^{7}	7.25×10^{-3}	41.8	3.54×10^{11}	29.1
62.7	2.07×10^{8}	1.38×10^{-2}	62.7	4.09×10^{11}	27.3
83.6	4.48×10^{8}	2.42×10^{-2}	83.6	4.69×10^{11}	25.3
104.5	9.02×10^{8}	3.97×10^{-2}	104.5	5.34×10^{11}	23.5
125.4	1.71×10^{9}	6.17×10^{-2}	125.4	6.03×10^{11}	21.8
	IM1 $\xrightarrow{k_6}$ $CH_2CClOH+H_2$			IM1 $\xrightarrow{k_6}$ $CH_2CClOH+H_2$	
0	4.45×10^{3}	5.89×10^{-7}	83.6	6.09×10^{5}	3.29×10^{-5}
20.9	1.99×10^{4}	2.07×10^{-6}	104.5	1.49×10^{6}	6.56×10^{-5}
41.8	7.24×10^{4}	5.96×10^{-6}	125.4	3.35×10^{6}	1.21×10^{-4}
62.7	2.24×10^{5}	1.49×10^{-5}			

DOI:10.1088/1674-0068/22/01/87-96

TABLE IV Microcanonical rate constants and branching ratios of the decompositions of IM2 for collision energies 0-125.4 kJ/mol

E_{col}	Rate constant/s^{-1}	Branching ratio/%	E_{col}	Rate constant/s^{-1}	Branching ratio/%
	IM2$\xrightarrow{k_{12}}$$CH_2ClCH_2O$+H			IM2$\xrightarrow{k_{16}}$$CClCH_2OH$+$H_2$	
0	2.43×10^{5}	2.75×10^{-4}	0	1.04×10^{7}	1.18×10^{-2}
20.9	6.81×10^{5}	4.78×10^{-4}	20.9	2.44×10^{7}	1.71×10^{-2}
41.8	1.70×10^{6}	7.97×10^{-4}	41.8	5.25×10^{7}	2.46×10^{-2}
62.7	3.86×10^{6}	1.22×10^{-3}	62.7	1.05×10^{8}	3.32×10^{-2}
83.6	8.10×10^{6}	1.77×10^{-3}	83.6	1.98×10^{8}	4.33×10^{-2}
104.5	1.59×10^{7}	2.46×10^{-3}	104.5	3.52×10^{8}	5.45×10^{-2}
125.4	2.95×10^{7}	3.31×10^{-3}	125.4	5.99×10^{8}	6.73×10^{-2}
	IM2$\xrightarrow{k_{13}}$$CH_2ClCHOH$+H			IM2$\xrightarrow{k_{17}}$$CH_2ClCHO$+$H_2$	
0	1.41×10^{8}	1.59×10^{-1}	0	8.97×10^{6}	1.01×10^{-2}
20.9	2.77×10^{8}	1.95×10^{-1}	20.9	1.75×10^{7}	1.23×10^{-2}
41.8	5.11×10^{8}	2.40×10^{-1}	41.8	3.21×10^{7}	1.51×10^{-2}
62.7	8.74×10^{8}	2.76×10^{-1}	62.7	5.59×10^{7}	1.77×10^{-2}
83.6	1.44×10^{9}	3.15×10^{-1}	83.6	9.31×10^{7}	2.03×10^{-2}
104.5	2.28×10^{9}	3.53×10^{-1}	104.5	1.49×10^{8}	2.31×10^{-2}
125.4	3.50×10^{9}	3.93×10^{-1}	125.4	2.30×10^{8}	2.58×10^{-2}
	IM2$\xrightarrow{k_{14}}$$CH_2ClCH_2$+OH			IM2$\xrightarrow{k_{18}}$$CH_2ClCH$+$H_2O$	
0	8.42×10^{9}	9.52	0	6.47×10^{8}	7.32×10^{-1}
20.9	1.46×10^{10}	10.3	20.9	1.15×10^{9}	8.08×10^{-1}
41.8	2.42×10^{10}	11.3	41.8	1.95×10^{9}	9.14×10^{-1}
62.7	3.85×10^{10}	12.2	62.7	3.16×10^{9}	9.99×10^{-1}
83.6	5.89×10^{10}	12.9	83.6	4.94×10^{9}	1.08
104.5	8.74×10^{10}	13.5	104.5	7.45×10^{9}	1.15
125.4	1.26×10^{11}	14.2	125.4	1.09×10^{10}	1.22
	IM2$\xrightarrow{k_{15}}$$CH_2Cl$+$CH_2OH$			IM2$\xrightarrow{k_{19}}$$CH_2CHOH$+HCl	
0	5.07×10^{10}	57.3	0	2.85×10^{10}	32.2
20.9	8.53×10^{10}	59.9	20.9	4.10×10^{10}	28.8
41.8	1.29×10^{11}	60.5	41.8	5.75×10^{10}	27.0
62.7	1.95×10^{11}	61.6	62.7	7.87×10^{10}	24.9
83.6	2.87×10^{11}	62.7	83.6	1.05×10^{11}	22.9
104.5	4.10×10^{11}	63.5	104.5	1.38×10^{11}	21.4
125.4	5.70×10^{11}	64.0	125.4	1.79×10^{11}	20.1

10^7-10^8 s^{-1}. From Fig.4, we can see that the rate constant of H formation channels is about five times larger than that of H_2 and the rate constants of the formation of HCl, OH, and H_2O are all between those of the formation of H_2 and CH_2OH. It is obvious in Fig.4 that the branching ratio of the formation of CH_2OH is the highest (57.3% at E_{col}=0) followed by HCl (32.2%). Therefore, at the collision energy of 0, the major products are CH_2OH and HCl with the branching ratio of about 1.8:1 between them. The branching ratios of the formations of H, H_2, H_2O, OH, and CH_2OH increase with the collision energy except for that of HCl, which decreases with the collision energy. The branching ratios of H, H_2, and H_2O change from 0.16%, 0.02%, and 0.7% to 0.40%, 0.09%, and 1.22%, respectively, but these channels remain minor ones. The branching ratio of OH increases from 9.52% to 14.2%. However, the branching ratio of the formation of HCl decreases from 32.2% to 20.1% when E_{col} changes from 0 to 125.4 kJ/mol. From Fig.4, we can see that the formations of HCl and OH become competing as the collision energy increases. At the collision energy of 125.4 kJ/mol, the branching ratios of CH_2OH and HCl are 64.0% and 20.1%, respectively, with the ratio of 3.2:1 between them. The ratio of the branching ratios of CH_2OH and HCl increases by a factor of 1.8. In summary, the main product of the decomposition of IM2 is CH_2OH both at low and high collision energies followed by HCl. However, OH starts

DOI:10.1088/1674-0068/22/01/87-96

to compete with HCl with the increase of the collision energy. The minor products of IM2 are H, H_2, and H_2O.

Since IM1 is more stable than IM2, the formation of IM1 is easier than that of IM2. Based on the above analysis, the main product of the $O(^1D)$+C_2H_5Cl reaction is probably HCl. Our results may give insight into reaction mechanisms and provide probable explanations for future experiments, but we feel that the description of these systems is yet incomplete and more work is needed for their full elucidation.

IV. CONCLUSION

The reaction of $O(^1D)$ with C_2H_5Cl was studied by QCISD(T)/6-311++G(d,p)//MP2/6-31G(d,p) theory. The calculations reveal an insertion-elimination mechanism. The association of $O(^1D)$ with C_2H_5Cl is found to be a barrierless reaction forming two energy-rich intermediates IM1 and IM2. Various decomposition reaction channels of IM1 and IM2 are reported. The energy-specific rate constants calculated by RRKM theory and the branching ratios of products show that HCl is the main product of IM1 and that CH_2OH is the main product of IM2. Since IM1 is more stable than IM2, the main product of $O(^1D)$+C_2H_5Cl reaction is HCl.

V. ACKNOWLEDGMENT

This work was supported by the National Natural Science Foundation of China (No.50772107).

[1] B. S. Wang, H. Hou, and Y. S. Gu, Chem. Phys. Lett. **304**, 278 (1999).
[2] S. Sekusak, H. Gusten, and A. Sabljic, J. Chem. Phys. **102**, 7504 (1995).
[3] F. G. Simone, J. P. Burrows, W. Schneider, G. K. Moortgat, and P. Grutzen, J. Phys. Chem. **93**, 7807 (1989).
[4] W. B. DeMore, J. Geophys. Res. **96**, 4995 (1991).
[5] Y. Tian, T. J. He, L. He, F. C. Liu, and D. M. Chen, Chin. J. Chem. Phys. **21**, 32 (2008).
[6] Y. D. Gao, L. S. Pei, Y. Chen, and C. X. Chen, J. Chem. Phys. **114**, 10798 (2001).
[7] Y. Yang, W. J. Zhang, S. X. Pei, J. Shao, W. Huang, and X. M. Gao, Chin. J. Chem. Phys. **18**, 908 (2005).
[8] Y. D. Gao, Y. Chen, X. X. Ma, and C. X. Chen, Chem. Phys. **269**, 389 (2001).
[9] F. Helleis, J. N. Crowley, and G. K. Moortgat, Geophys. Res. Lett. **21**, 1795 (1994).
[10] X. G. Zhou, J. Li, X. Zhao, Y. Tian, L. M. Zhang, Y. Chen, C. X. Chen, S. Q. Yu, and X. X. Ma, Phys. Chem. Chem. Phys. **3**, 3662 (2001).
[11] P. Piggs, C. E. Canosa-Mas, J. M. Fracheboud, G. Marston, D. E. Shallcross, and R. P. Wayne, J. Chem. Soc. Faraday Trans. **91**, 3045 (1995).
[12] J. Espinosa-Garcia, Chem. Phys. Lett. **316**, 563 (2000).
[13] T. Jungkamp, A. Kukui, and R. N. Schindler, Ber Bunsen-Ges Phys. Chem. **99**, 1057 (1995).
[14] J. N. Crowley, P. Campuzano-Jost, and G. K. Moortgat, J. Phys. Chem. **100**, 3601 (1996).
[15] S. Li, Z. S. Li, J. Y. Liu, J. F. Xiao, and C. C. Sun, J. Comput. Chem. **25**, 72 (2004).
[16] H. Q. He, J. Y. Liu, Z. S. Li, and C. C Sun, J. Mol. Struct.: THEOCHEM **763**, 59 (2004).
[17] M. Alagia, N. Balucani, and P. Casavecchia, Chem. Phys. Lett. **258**, 323 (1996).
[18] T. L. Nguyen, A. M. Mebel, and S. H. Lin, J. Chem. Phys. **114**, 10816 (2001).
[19] T. J. He, D. M. Chen, F. C. Liu, and L. S. Sheng, Chem. Phys. Lett. **332**, 545(2002).
[20] Y. C. Sun, I. T. Wang, T. L. Nguyen, H. F. Lu, X. M. Yang, and A. M. Mebel, J. Phys. Chem. A **107**, 6986 (2003).
[21] W. J. Hehre, L.Radom, and P. V. R. Schleyer, *Ab initio Molecular Orbital Theory*, New York: John Wiley, (1986).
[22] M. J. Frisch, G. W. Trucks, H. B. Schlegel, G.E. Scuseria, M. A. Robb, J. R. Cheeseman, J. A. Montgomery, Jr., T. Vreven, K. N. Kudin, J. C. Burant, J. M. Millam, and S. S. Iyengar, *Gaussian 03*, Pittsburgh, PA: Gaussian, Inc., (2003).
[23] P. J. Robinson and K. A. Holbrook, *Unimolecular Reactions*, New York: Wiley, (1972).
[24] J. I. Steinfeld, J. S. Francisco, and W. L. Hase, *Chemical Kinetics and Dynamics*, Englewood Cliffs: Prentice-Hall, (1999).
[25] H. S. Tam, J. H. Choe, and M. D. Harmony, J. Phys. Chem. **95**, 9267 (1991).
[26] K. P. Humer and G. Herzberg, *Molecular Spectra and Molecular Structure. IV. Constants of Diatomic Molecules*, New York: Van Nostrand Reinhold Co., 284 (1979).
[27] D. R. Lide, *CRC Handbook of Chemistry and Physics*, 73rd Ed, Boca Raton: CRC Press, (1992).
[28] M. W. Chase, Jr., C. A. Davies, J. R. Downey, Jr., D. J. Frurip, R. A. McDonald, and A. N. Syverud, *JANAF Thermochemical Tables*, Vol.14. 3rd, Washington: National Bureau of Standards, (1985).
[29] M. D. Harmony, J. Chem. Phys. **93**, 7522 (1990).

DOI:10.1088/1674-0068/22/01/87-96